THE JOURNAL OF BIOLOGICAL CHEMISTRY VOL. 284, NO. 24, pp. 16236–16245, June 12, 2009

Oxygen Sensitivity of Mitochondrial Reactive Oxygen Species Generation Depends on Metabolic Conditions[S]

Received for publication, December 18, 2008, and in revised form, March 18, 2009 Published, JBC Papers in Press, April 14, 2009, DOI 10.1074/jbc.M809512200

David L. Hoffman[‡] **and Paul S. Brookes**[§1]

From the Departments of [‡]*Biochemistry and* [§]*Anesthesiology, University of Rochester Medical Center, Rochester, New York 14642*

The mitochondrial generation of reactive oxygen species (ROS) plays a central role in many cell signaling pathways, but debate still surrounds its regulation by factors, such as substrate availability, [O_2] and metabolic state. Previously, we showed that in isolated mitochondria respiring on succinate, ROS generation was a hyperbolic function of [O_2]. In the current study, we used a wide variety of substrates and inhibitors to probe the O_2 sensitivity of mitochondrial ROS generation under different metabolic conditions. From such data, the apparent K_m for O_2 of putative ROS-generating sites within mitochondria was estimated as follows: 0.2, 0.9, 2.0, and 5.0 μM O_2 for the complex I flavin site, complex I electron backflow, complex III Q_O site, and electron transfer flavoprotein quinone oxidoreductase of β-oxidation, respectively. Differential effects of respiratory inhibitors on ROS generation were also observed at varying [O_2]. Based on these data, we hypothesize that at physiological [O_2], complex I is a significant source of ROS, whereas the electron transfer flavoprotein quinone oxidoreductase may only contribute to ROS generation at very high [O_2]. Furthermore, we suggest that previous discrepancies in the assignment of effects of inhibitors on ROS may be due to differences in experimental [O_2]. Finally, the data set (see supplemental material) may be useful in the mathematical modeling of mitochondrial metabolism.

The production of reactive oxygen species (ROS)[2] by mitochondria has been implicated in numerous disease states, including but not limited to sepsis, solid state tumor survival, and diabetes (1). In addition, mitochondrial ROS (mtROS) play key roles in cell signaling (reviewed in Refs. 2 and 3). There exist within mitochondria several sites for the generation of ROS, with the most widely studied being complexes I and III of the electron transport chain (ETC). However, there is currently some debate regarding the relative contribution of these complexes to overall ROS production (4–9) and the factors that may alter this distribution. One such factor considered herein is [O_2]. Estimates of physiological [O_2] within tissues (*i.e.* interstitial [O_2]) range from 37 down to 6 μM at 5–40 μm away from a blood vessel (10). More recently, EPR oximetry has estimated tissue [O_2] to be in the 12–60 μM range (11). In addition, elegant studies with hepatocytes have shown that O_2 gradients exist within cells, such that an extracellular [O_2] of 6–10 μM yields an [O_2] of ~5 μM close to the plasma membrane, dropping to 1–2 μM close to mitochondria deep within the cell (12). In cardiomyocytes, at an extracellular [O_2] of 29 μM, intracellular [O_2] varied in the range 6–25 μM (13). Clearly, different tissues consume O_2 at different rates, so these gradients can vary considerably between tissue and cell types.

By definition, the generation of reactive *oxygen* species by any mechanism, is an O_2-dependent process. However, measurements in intact cells have indicated that mtROS generation increases at lower O_2 levels (1–5% O_2) (14). Proponents of an increase in mtROS in response to hypoxia suggest that under such conditions, reduction of the ETC results in increased leakage of electrons to O_2 at the Q_O site of complex III (14). Such a model posits that increased hypoxic ROS is a mitochondria-autonomous signaling mechanism (*i.e.* it is an inherent property of the mitochondrial ETC). Therefore, mtROS generation should increase in hypoxia regardless of the experimental system being studied, including isolated mitochondria. In contrast to this hypothesis, we and others have demonstrated that ROS generation by mitochondria is a positive function of [O_2] across a wide range of values (0.1–1000 μM O_2) (15–18), suggesting that signaling mechanisms external to mitochondria may be required to facilitate the increased hypoxic mtROS production observed in cells.

One limitation of our previous work (15) was that only a single respiratory condition was studied, namely succinate as respiratory substrate (feeding electrons into complex II) plus rotenone to inhibit backflow of electrons through complex I (5, 7). The possibility exists that under different metabolic conditions, which may lead to differential redox states between the cytochromes in the ETC (19, 20), ROS generation may exhibit a different response to [O_2]. Thus, in the current study, we examined the response of mtROS generation to [O_2] under 11 different conditions, using a variety of respiratory substrates and inhibitors (for a thorough review of electron entry points to the ETC under various substrate/inhibitor combinations, see Ref. 21). Fig. 1 shows a schematic of the mitochondrial ETC, highlighting sites of electron entry resulting from various substrates, binding sites of inhibitors, and major sites of ROS generation. Fig. 2 shows the specific details of each experimental condition, indicating the predicted sites of ROS generation resulting from the use of each substrate/inhibitor combination. The legend to Fig. 2 provides an explanation of each condition.

[S] The on-line version of this article (available at http://www.jbc.org) contains supplemental Tables S1–S3.

[1] To whom correspondence should be addressed: Box 604, Dept. of Anesthesiology, University of Rochester Medical Center, 601 Elmwood Ave., Rochester, NY 14642. Tel.: 585-273-1626; Fax: 585-273-2652; E-mail: paul_brookes@urmc.rochester.edu.

[2] The abbreviations used are: ROS, reactive oxygen species; mtROS, mitochondrial ROS; ETC, electron transport chain; ETFQOR, electron transfer flavoprotein quinone oxidoreductase.

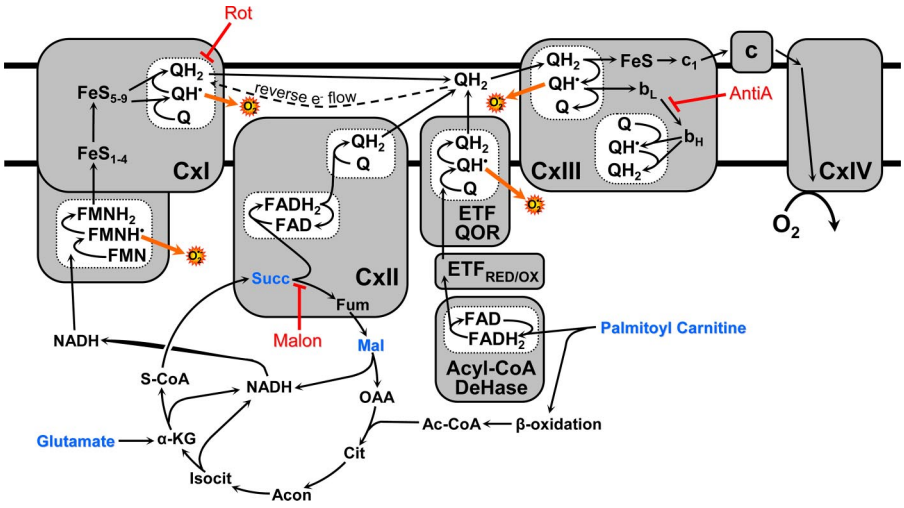

FIGURE 1. **Mitochondrial pathways of electron flow resulting from the substrates and inhibitors used in this study.** Substrates used were glutamate/malate (which generates NADH via the tricarboxylic acid cycle, feeding into complex I), succinate (which feeds electrons directly into complex II), and palmitoyl-carnitine (which feeds electrons into the ETC via acyl-CoA dehydrogenase as well as through the β-oxidation pathway). (For a more thorough explanation, refer to Ref. 21.) Inhibitors used were rotenone (which inhibits at the downstream Q binding site of complex I (9)), malonate (a competitive inhibitor of complex II (25, 26)), and antimycin A (a complex III inhibitor that prevents electron flow to the Q_i site of complex III, thus stabilizing $QH^{\bullet}$ at the Q_O site (6, 28)).

The results of these studies indicated that although ROS generation under all experimental conditions exhibited the same overall response to $[O_2]$ (*i.e.* hyperbolic, with decreased ROS at low $[O_2]$), the apparent K_m for O_2 varied widely between metabolic states.

EXPERIMENTAL PROCEDURES

All chemicals were the highest grade available from Sigma unless otherwise indicated. Male adult Sprague-Dawley rats (250 g) were purchased from Harlan (Indianapolis, IN) and were maintained in accordance with Ref. 53. All procedures were approved by the University of Rochester Committee on Animal Resources (protocol number 2007-087). Liver mitochondria were isolated by differential centrifugation, as described previously (15).

Mitochondrial incubations were performed using an open flow respirometry cell, as described previously (15, 22). Briefly, mitochondria were suspended in the liquid phase in a stirred chamber with a head space gas of tightly controlled pO_2 flowing above. Such a system, in which the liquid phase $[O_2]$ is measured with an O_2 electrode, permits prolonged mitochondrial incubation at tightly controlled steady-state $[O_2]$ and the calculation of mitochondrial O_2 consumption by a simplified Fick equation (15, 22, 23). The O_2 electrode was calibrated daily with air-saturated deionized H_2O, with or without sodium dithionite. The impact of additions to mitochondrial incubations (*e.g.* substrates or inhibitors) on O_2 solubility was no more than 0.4% of the total. A fiber optic fluorimeter was built into the chamber, permitting measurement of mitochondrial ROS generation using the H_2O_2-sensitive dye Amplex red (23). Authentic H_2O_2 was added at the end of each experimental run to internally calibrate the fluorescent signal. Such a method ensures that the obtained signal truly reflects the net H_2O_2 production and is not affected by scavenging due to enzymes, such as catalase.

Incubations were carried out in mitochondrial respiration buffer (15), with oligomycin (1 μg/ml) present to enforce state 4 respiration. Where indicated, mitochondrial substrates and inhibitors were used at the following concentrations: glutamate (10 mM), malate (5 mM), succinate (10 mM), palmitoyl-carnitine (1 μM), rotenone (1 μM), antimycin A (10 μM), malonate (2 mM). They were present from the beginning of incubations before mitochondrial addition. Superoxide dismutase (80 units/ml) was present in all incubations to ensure rapid dismutation of $O_2^{\bullet-}$ to H_2O_2 and to avoid scavenging of the former by reaction with nitric oxide ($NO^{\bullet}$). This was a precaution, despite our previous observations that additional superoxide dismutase was not necessary in this regard and that $NO^{\bullet}$ scavenging of $O_2^{\bullet-}$ (which would lead to peroxynitrite-mediated tyrosine nitration) was not occurring in hypoxia (15). The latter is also unlikely because the K_m for O_2 of all NOS isoforms is very high (6–24 μM) (24), so $NO^{\bullet}$ generation actually decreases in hypoxia. Full details on each combination of substrates/inhibitors and the putative sites of ROS generation resulting from each are given under "Results" and in the legends to Figs. 1 and 2.

The steady-state $[O_2]$ reached in open flow respirometry is not an independent variable but a result of the individual characteristics of each mitochondrial incubation. Therefore, it is not possible to use the raw data to calculate average rates of ROS generation at a single $[O_2]$. Thus, for each metabolic condition, the empirical values of ROS generation across a range of steady-state $[O_2]$ (typically 7–10 points/curve) were fitted to a single-substrate binding curve, employing Prism software (GraphPad, San Diego, CA), as described previously (15). The curve fit parameters (V_{max}, K_m) were then used to extrapolate ROS generation rates at common values of $[O_2]$, and these data then averaged between individual experiments ($n \geq 5$).

RESULTS

State 4 respiration rates (VO_2; nmol of O_2/min/mg of protein) under each metabolic condition were calculated across the range of $[O_2]$ values studied, as previously described (15, 22). The maximal VO_2 (at high $[O_2]$) for each condition is listed in each *panel* of Fig. 2, whereas the full response curves of VO_2 to $[O_2]$ are in Table S1. VO_2 varied considerably between metabolic substrates. For example, a higher VO_2 was observed with complex II substrates (condition E) than with complex I substrates (condition A). The consensus view is that because fewer H^+ are pumped across the inner membrane when electrons enter at complex II, the ETC has to work faster in condition E (and thus consume more O_2) to maintain the same H^+ gradient as in condition A.

The generation of ROS as a function of $[O_2]$ for metabolic conditions A–L (Fig. 2) is illustrated in Fig. 3. Respiring on

complex I-linked substrates (glutamate plus malate in the presence of malonate to inhibit complex II), ROS generation was maximal at 250 pmol/min/mg mitochondrial protein, whereas K_m was 0.25 μM O_2 (Fig. 3*A*). As expected, the addition of rotenone, which inhibits at the downstream Q site of complex I, increased maximal ROS slightly (V_{max} 295) while causing a right shift in the curve (K_m = 2.0 μM O_2; Fig. 3*B*). Similarly, inhibition at complex III by antimycin A also increased ROS (V_{max} 460) and further right-shifted the curve (K_m = 5.0 μM O_2; Fig. 3*C*).

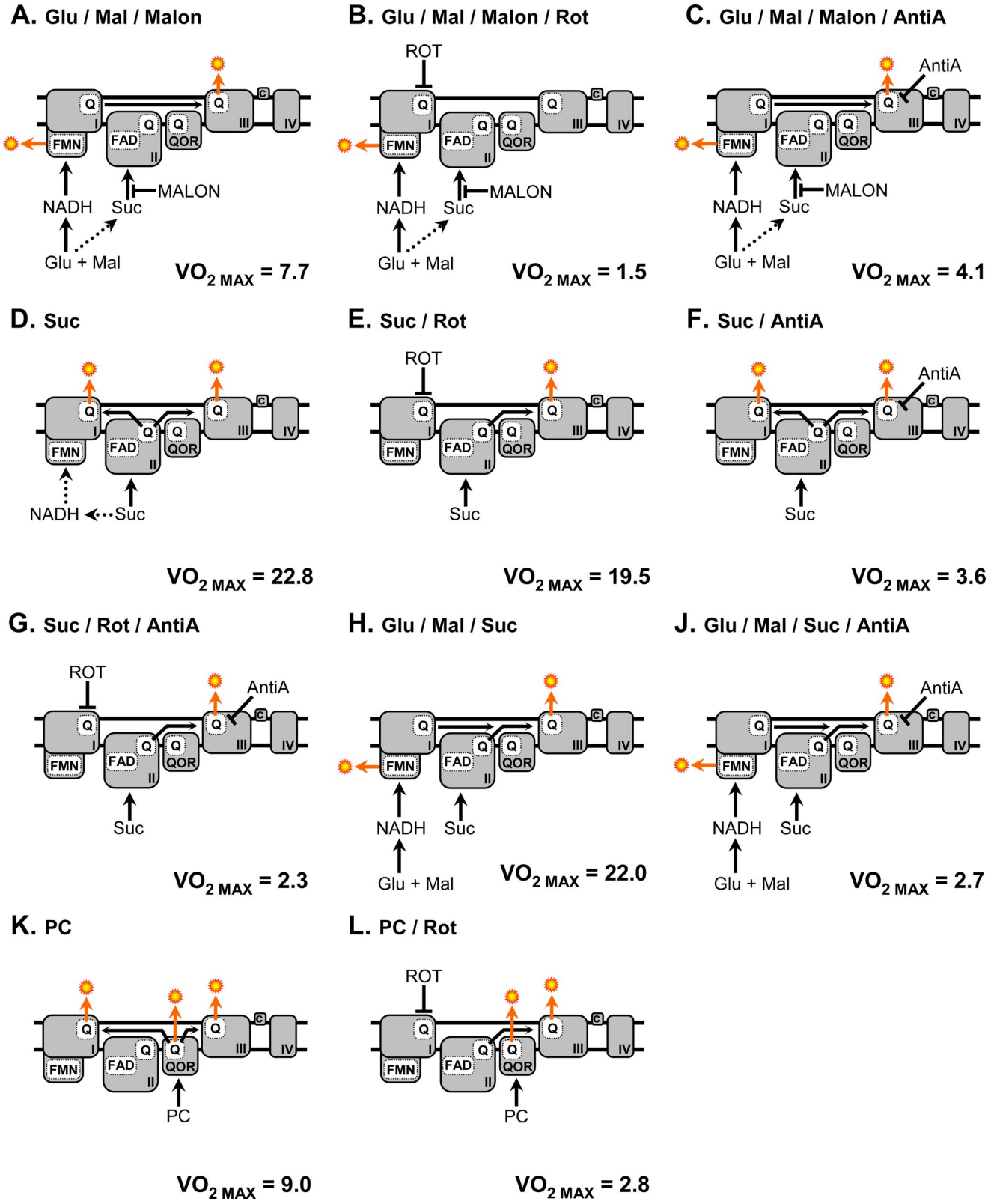

With succinate as the respiratory substrate, feeding electrons into complex II (Fig. 3*D*), maximal ROS generation was 330 pmol/min/mg mitochondrial protein with a K_m of 1.8 μM O_2. Some of this ROS was due to backflow of electrons through complex I, since the addition of rotenone (Fig. 3*E*) brought the V_{max} value down to 105 and the K_m to 0.7 μM O_2. Similarly to the situation with complex I-linked substrates (see above), the addition of antimycin A to succinate-respiring mitochondria (Fig. 3*F*) raised maximal ROS generation to 420 pmol/min/mg mitochondrial protein and strongly right-shifted the curve (K_m = 12 μM O_2). Adding both rotenone and antimycin A together (Fig. 3*G*) gave a V_{max} of 380 and a K_m of 4 μM O_2. Thus, in both complex I- and II-linked respiration, antimycin A-induced ROS generation is heavily O_2-dependent, having a much greater K_m than base-line ROS generation (Fig. 3, *C versus A*, *G versus E*, and *F versus D*).

Under conditions of dual electron entry at complexes I and II (*i.e.* respiration on glutamate, malate, and succinate together) (Fig. 3*H*), maximal ROS generation was 330 pmol/min/mg mitochondrial protein, and K_m was 0.5 μM O_2. As seen for complex I- or complex II-linked substrates alone, the addition of antimycin A to the dual electron entry condition (Fig. 3*J*) resulted in the highest ROS generation measured under any condition (V_{max} = 490) and a strongly right-shifted curve (K_m = 9 μM O_2).

In mitochondria respiring on palmitoyl-carnitine, maximal ROS was 290 pmol/min/mg mitochondrial protein, with a K_m of 1.0 μM O_2. Similar to the situation with complex II, some of this ROS may result from complex I backflow, since the addition of rotenone resulted in a decrease in ROS (V_{max} = 250) and a right shift in the curve (K_m = 4 μM O_2).

DISCUSSION

In the current study, we examined the response of mtROS generation to [O_2] under 11 different conditions, using a variety of respiratory substrates and inhibitors (Fig. 2, *A–L*). Fig. 3 shows mtROS generation as a function of [O_2] for each of the 11 conditions A–L. In conditions A–C, electrons entered the ETC at complex I, with complex II blocked by malonate (25, 26). In conditions D–G, electrons entered at complex II. In conditions H and J, electrons entered at both complexes I and II, and in conditions K and L, electrons entered at the β-oxidation electron transfer flavoprotein quinone oxidoreductase (ETFQOR). Despite the different sites of electron entry, all conditions exhibited the same overall pattern of ROS generation in response to [O_2], namely a hyperbolic function with lower ROS generation rate at lower [O_2]. Thus, it appears that our previous data set showing decreased mtROS at low [O_2] (15) was not an artifact of the metabolic conditions chosen (succinate plus rotenone).

Although information on ROS generation under different substrate/inhibitor conditions is useful in the field of isolated mitochondrial bioenergetics, it would be more useful to know the O_2 sensitivity of ROS generation from putative sites within the ETC. Thus, a series of calculations was devised to estimate ROS generation from each of four putative sites, at varying [O_2] (Fig. 4). Below, the rationale behind each calculation is discussed along with the results.

Complex III Q_O Site—The rate of ROS generation from the Q_O site of complex III was estimated by two methods. First, it was estimated by using the rate of ROS generation obtained in the presence of succinate as substrate (complex II) plus rotenone to inhibit electron backflow through complex I (*i.e.* condition E) (5, 9, 27). Under this condition, ROS generation occurs primarily at the complex III Q_O site (6, 7, 28). Second, the rate of ROS generation due to backflow of electrons through complex I (calculated below) was subtracted from the rate of ROS with succinate alone in which electrons flow both forward through complex III and backward through complex I (condition D). The two values for complex III Q_O site ROS generation were then averaged (Fig. 4*A*), resulting in a V_{max} of 150 and apparent K_m of 2.0.

Complex I FMN Site—To estimate ROS generation by the complex I FMN site, we used mitochondria respiring on complex I-linked substrates alone (*i.e.* glutamate plus malate) in the presence of a complex II inhibitor to prevent electron entry due to passage of substrates through the tricarboxylic acid cycle. The inhibitor chosen was malonate, since 2-thenoyltrifluoroacetone (29) exhibited an absorbance spectrum that interfered with Amplex Red (not shown) and may also stimulate ROS generation at complex II (30, 31). Under condition A (glutamate, malate, and malonate), some electron flux proceeds via the Q pool to complex III. Thus, it is necessary to subtract ROS generation by the complex III Q_O site. Furthermore, it is insufficient to merely subtract ROS as calculated above, since that

FIGURE 2. **Pathways of electron flow for the substrate/inhibitor combinations used in conditions A–L.** Each *panel* includes the respective maximal respiration rate ($VO_{2\ max}$; nmol of O_2/min/mg of protein) measured under each condition. *A*, glutamate/malate/malonate. Electrons enter through complex I, whereas electron entry at complex II is inhibited by malonate. ROS generation occurs at the FMN site of complex I as well as the Q_O site of complex III. *B*, glutamate/malate/malonate/rotenone. Electrons enter through complex I. Electron passage through complex I is inhibited by rotenone binding at the downstream Q site, resulting in maximal ROS production at the FMN site of complex I. ROS production at the Q_O site of complex III is prevented due to no electrons reaching the complex from either complexes I or II, both of which are inhibited. *C*, glutamate/malate/malonate/antimycin A. Electrons enter through complex I only, since complex II is blocked. Flow of electrons is inhibited by the complex III inhibitor antimycin A, resulting in ROS production at the Q_O site of complex III, as well as the FMN site of complex I. *D*, succinate. Electrons enter at complex II. ROS is generated by the flow of electrons though the Q_O site of complex III as well as the backflow of electrons through complex I. *E*, succinate/rotenone. Electrons enter at complex II, and ROS is generated at the Q_O site of complex III, because rotenone is present to inhibit backflow of electrons through complex I. *F*, succinate/antimycin A. Electrons enter through complex II. ROS is generated at both complex I via backflow and complex III Q_O, with an increased rate at the latter due to inhibition by antimycin A. *G*, succinate/rotenone/antimycin A. Electrons enter through complex II. Backflow of electrons through complex I is inhibited by rotenone, whereas ROS generation at complex III Q_O is augmented due to the presence of antimycin A. *H*, glutamate/malate/succinate. Electrons enter at both complexes I and II. ROS is generated from the complex I FMN site and the complex III Q_O site. *J*, glutamate/malate/succinate/antimycin A. Electrons enter at complexes I and II. ROS generation occurs at the complex I FMN and is augmented at the complex III Q_O site by antimycin A. *K*, palmitoyl-carnitine. Electrons enter at the ETFQOR. ROS is generated at the ETFQOR as well as complex I via backflow and at the complex III Q_O site. *L*, palmitoyl-carnitine/rotenone. Electron entry is at the ETFQOR. ROS is generated at the ETFQOR as well as at the complex III Q_O site, whereas ROS due to complex I backflow is blocked by rotenone. *Glu*, glutamate; *Mal*, malate; *Suc*, succinate; *PC*, palmitoyl-carnitine; *Rot*, rotenone; *AntiA*, antimycin A; *Malon*, malonate.

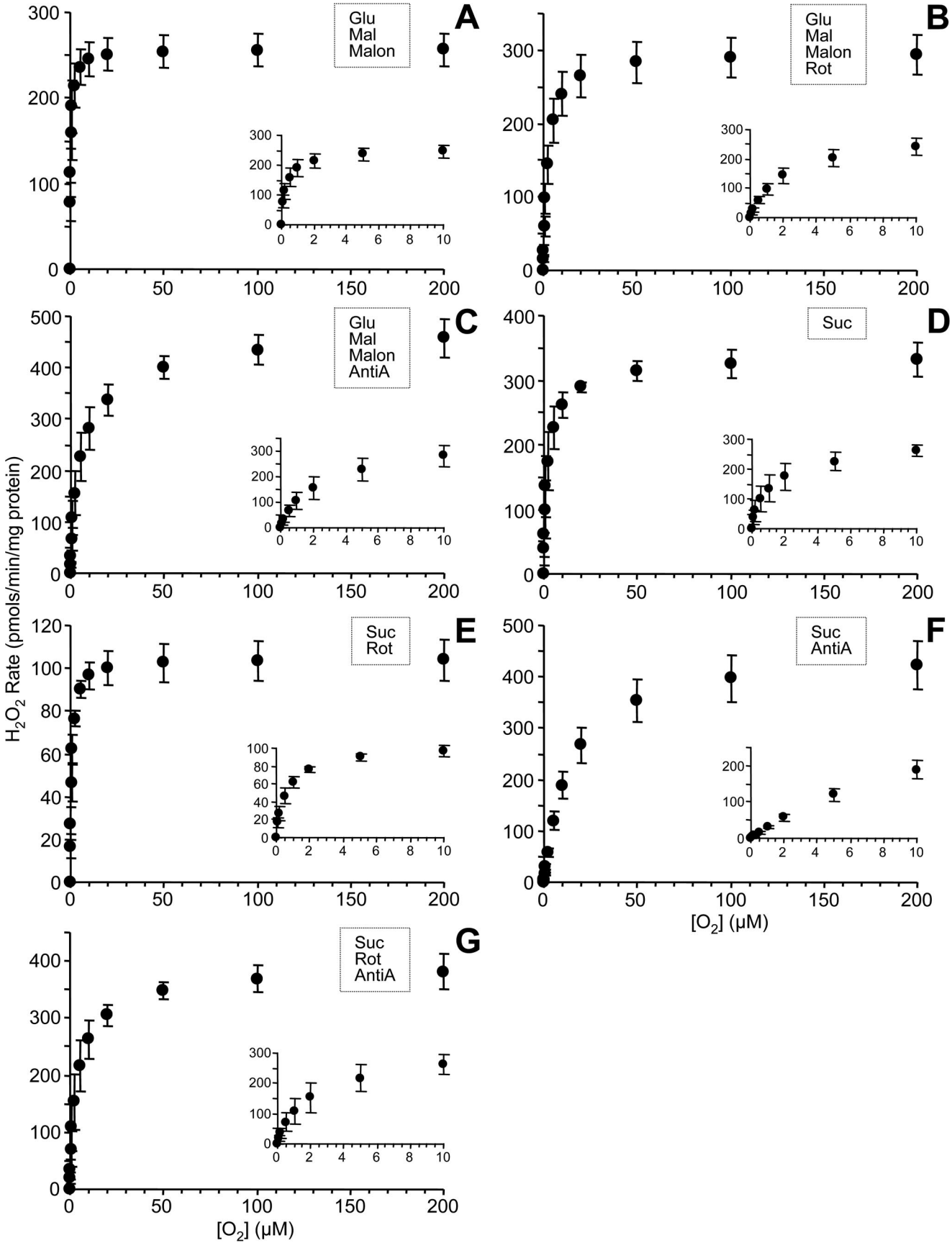

FIGURE 3. **O_2 response of ROS generation rate for different substrate inhibitor combinations.** ROS generation by isolated rat liver mitochondria under different steady state $[O_2]$ for conditions A–L as detailed in Fig. 2. The substrate/inhibitor combination utilized in each condition is also indicated on each *graph*. Data are means ± S.E. ($n \geq 5$).

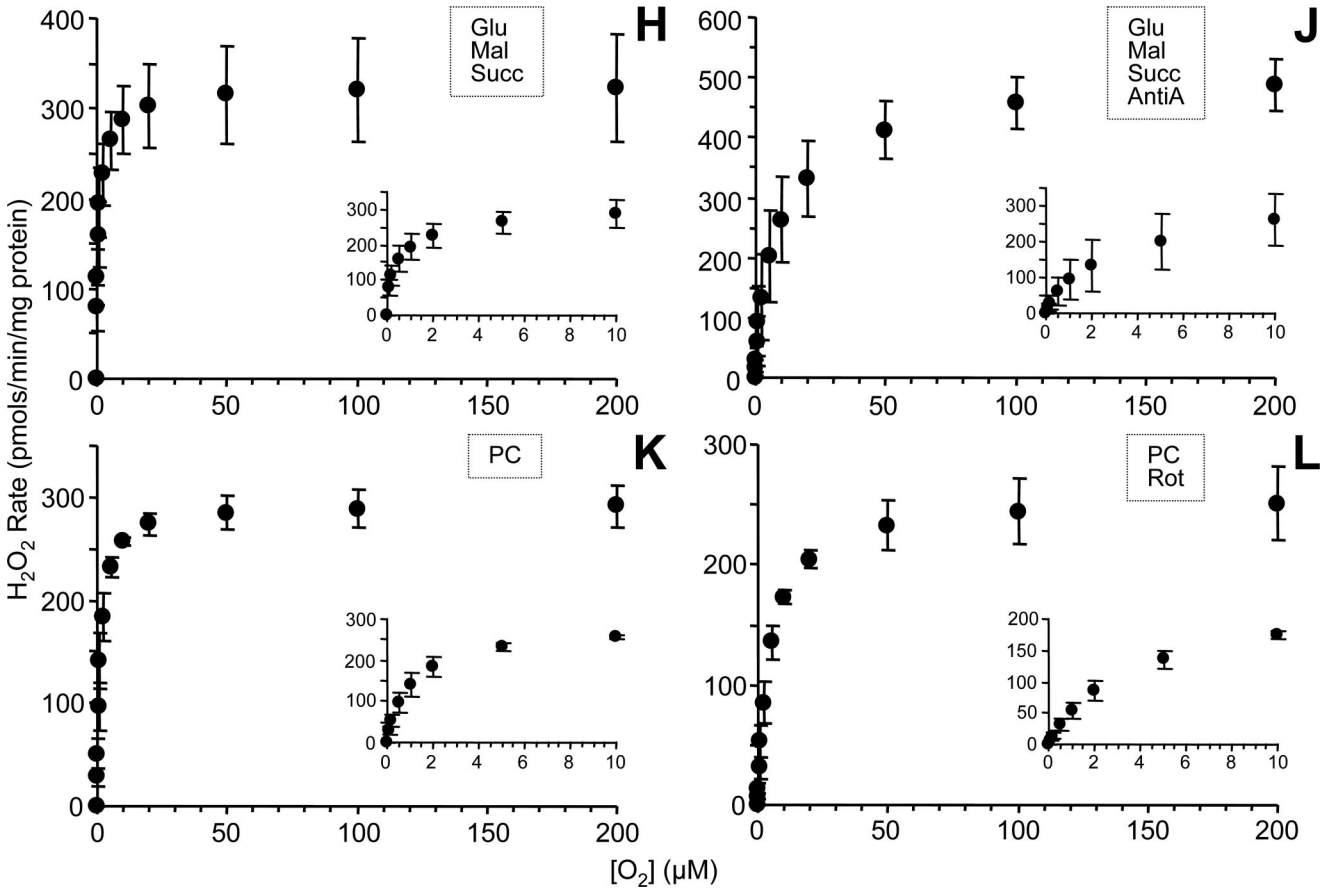

FIGURE 3— *continued*

flux was calculated from mitochondria respiring on succinate, and the flux through the respiratory chain (*i.e.* VO_2) was lower with glutamate plus malate. This lower electron flux has two opposing effects on ROS generation by complex III Q_O. First, fewer electrons reach complex III, as shown by the VO_2 in condition A (Fig. 2*A*), which was 39.3% of that in condition E (Fig. 2*E*). Second, this slower electron flux through complex III results in an increased dwell time for the ubisemiquinone radical at the Q_O site, which enhances ROS generation (32). To correct for this second effect, it is necessary to determine the relationship between the percentage of electrons diverted to ROS and the total electron flux (VO_2). Fig. 5 shows this relationship for mitochondria respiring in condition E (succinate plus rotenone), indicating that a VO_2 of 19.5 nmol of O_2/min/mg results in 1.065% of electrons going to ROS. Lowering the VO_2 to 7.7 (*i.e.* the VO_2 in condition A) increases this value to 1.817%. Thus, the percentage of electrons diverted to ROS is 1.71-fold greater in condition A *versus* condition E. Combining these two correction factors (39.3% × 1.71) indicates that it is necessary to subtract 67.2% of the ROS from the complex III Q_O site (Fig. 4*A*) to reveal the residual ROS from the complex I FMN site. The result is shown in Fig. 4*B*, and interestingly, the shape of the curve is not a classical hyperbolic function but instead indicates a V_{max} of 170 at 5 μM O_2, with ROS declining very slightly at higher $[O_2]$. The apparent K_m from this curve was estimated as 0.19 μM O_2. These data therefore suggest that the complex I FMN site is able to generate ROS at O_2 levels far below that at which the complex III Q_O site is already O_2-limited (K_m = 2.0 μM O_2; see Fig. 4*A*).

Notably, Fig. 5, which shows that the percentage of electron flux diverted to ROS increases as respiration slows down, might be misconstrued as demonstrating that mitochondrial ROS generation increases at low respiration rates (such as those caused by low $[O_2]$). However, as we previously discussed (15), although a greater percentage of electrons may be diverted to ROS, the absolute number of electrons flowing through the respiratory chain and thus available for diversion decreases by a far greater magnitude, such that the absolute number of ROS generated is lower. From both ROS detection and cell signaling perspectives, the parameter that matters is not the percentage of electrons diverted to ROS but the absolute amount of ROS, which always decreases at low $[O_2]$.

Complex I Backflow—The backflow of electrons through complex I causes ROS production at its downstream ubiquinone binding site (5, 9), which can be calculated in two ways. First, ROS generation in the presence of succinate alone (condition D) includes ROS from both forward and backward electron flow. The contribution of backflow can be quantified by subtracting data obtained under the forward flow only condition (*i.e.* succinate plus rotenone, condition E). Second, palmitoyl-carnitine feeding electrons into the Q-pool can serve as an alternative source of electrons for complex I backflow. Similarly to the succinate data (condition D *versus* E), the presence or absence of rotenone to prevent backflow can also be applied to

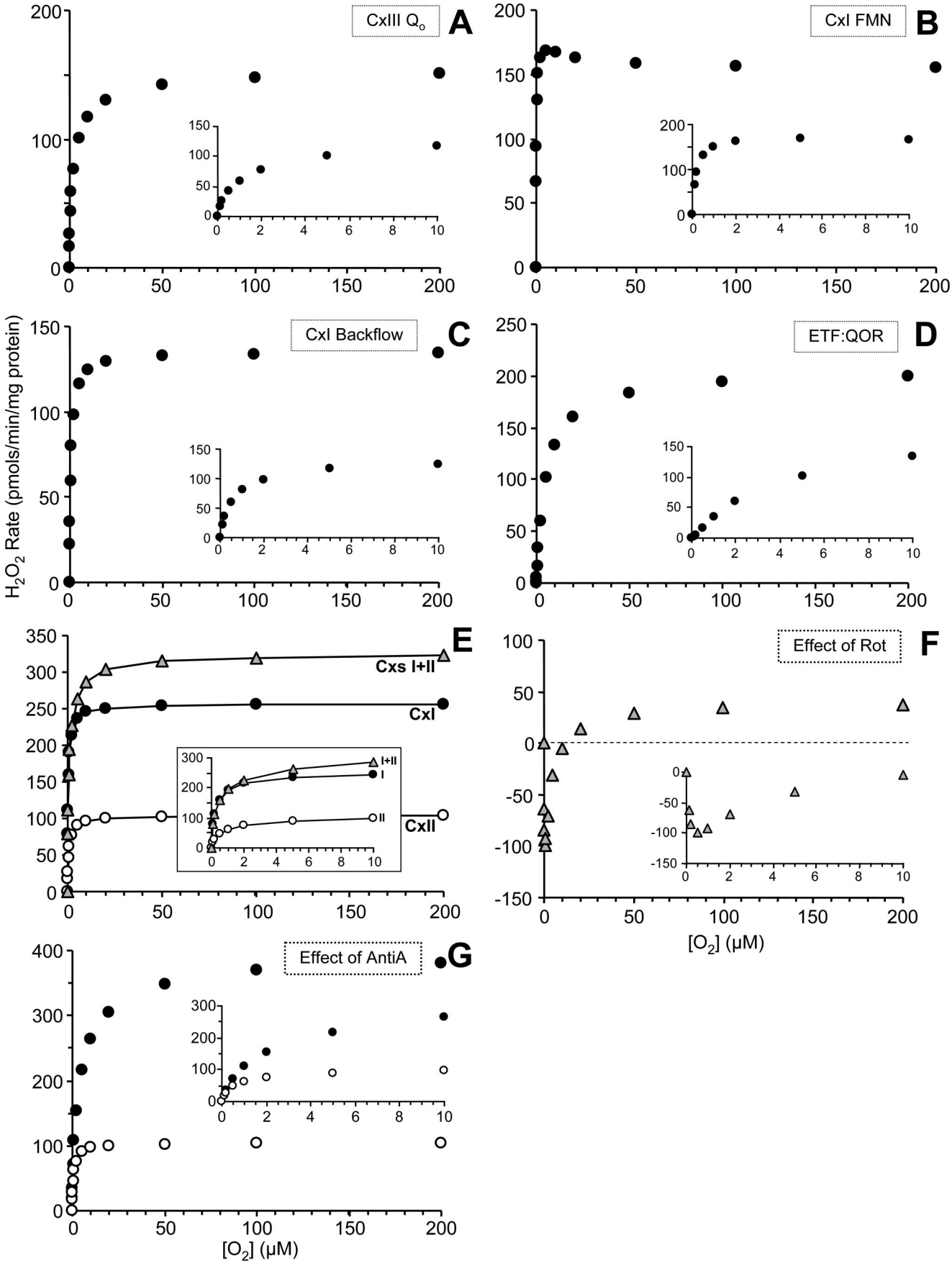
CxIII Q$_o$
A
CxI FMN
B
CxI Backflow
C
ETF:QOR
D
H$_2$O$_2$ Rate (pmols/min/mg protein)
Cxs I+II
CxI
CxII
I+II
I
II
E
Effect of Rot
F
[O$_2$] (μM)
Effect of AntiA
G
[O$_2$] (μM)

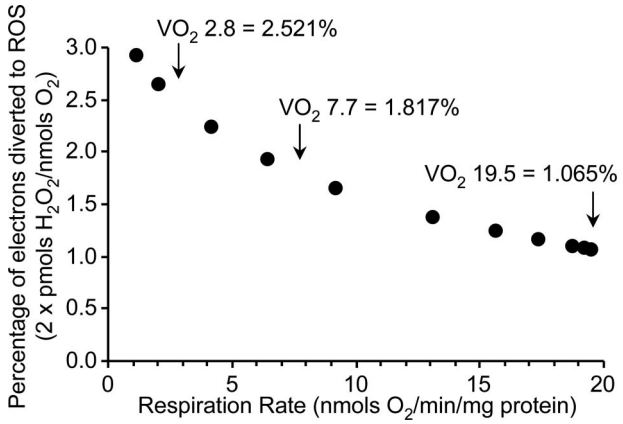

FIGURE 5. **ROS generation as a percentage of electron flux through the respiratory chain, as a function of respiration rate (VO_2).** Two molecules of $O_2^{\cdot-}$ are required to make one H_2O_2, so data on the *y* axis were calculated by dividing 2 × ROS generation rate by the respiration rate. Data are from mitochondria respiring on succinate plus rotenone (condition E) and are taken from the tables in the supplemental material. Error bars are eliminated for clarity. The *right-most point* is state 4 respiration, with the remaining *points* on the curve originating from changes in VO_2 due to titration of O_2 levels. The *arrows* highlight specific values of VO_2 referred to throughout and the extrapolated values of percentage of electrons diverted to ROS.

palmitoyl-carnitine-linked ROS generation (*i.e.* condition K *versus* L) to infer the rate of ROS from backflow. Averaged data from these two calculations are shown in Fig. 4*C*, indicating a V_{max} of 135 and an apparent K_m of 0.9 μM O_2. The occurrence and physiological importance of ROS from complex I backflow remains unclear (5, 7, 9), and the data in Fig. 4*C* indicate the importance of $[O_2]$ in regulating this phenomenon. In addition, the ratio of complex I *versus* complex II substrates is expected to play an important regulatory role *in vivo*, since forward electron flow through complex I will effectively prohibit backflow (21, 33, 34).

ETFQOR—The ETFQOR of β-oxidation is known to generate ROS (5). In the presence of palmitoyl-carnitine (condition K) ROS generation is from three sites: the ETFQOR, complex III Q_O site, and complex I backflow. To account for backflow, it is necessary to consider the rate of palmitoyl-carnitine-linked ROS generation in the presence of rotenone (condition L). To account for ROS from the complex III Q_O site under these conditions, a similar calculation is performed as above for the complex I FMN site (*i.e.* scaling of the complex III Q_O site data using a correction factor that considers the effects of respiration rate on ROS generation at this site). Electron flux through complex III in the presence of palmitoyl-carnitine plus rotenone (VO_2 = 2.8; Fig. 2*L*) is 14.3% of the flux with succinate plus rotenone (VO_2 = 19.5; Fig. 2*E*). Furthermore, by reference to Fig. 5, this lower electron flux results in a 2.37-fold increase in the percentage of electrons donated to ROS (*versus* that observed at maximal flux). Combining these correction factors, it is necessary to subtract 34% of the ROS generation from the complex III Q_O site (condition E) to reveal the residual ROS from the ETFQOR. Data from this calculation are shown in Fig. 4*D*, indicating a V_{max} of 200 and an apparent K_m of 5 μM O_2. Thus, although these data are consistent with the proposal that the ETFQOR can be a significant source of ROS (5), the high apparent K_m indicates that this may only occur at high $[O_2]$.

Dual Electron Entry—mtROS generation in the presence of both complex I- and II-linked substrates (condition H) was very high (V_{max} = 330), with a K_m of 0.5 μM O_2. As visualized in Fig. 4*E*, above 5 μM O_2, the ROS generation was almost additive between the two individual substrate conditions (*i.e.* ROS with complex I substrates plus ROS with complex II substrates = ROS with both complex I and II substrates). This suggests that at high $[O_2]$, some spare capacity exists in the ROS-generating system, such that adding more electrons from either complex I or II can increase ROS generation. Thus, at high $[O_2]$, the mix of substrates may profoundly impact on the rate of ROS generation. However, interestingly at lower $[O_2]$ (below 2 μM; Fig. 4*E*, *inset*), the ROS generation rate under dual electron entry closely matched the rate with complex I substrates alone (*i.e.* adding electrons from complex II did not increase the rate of ROS generation). This suggests that at low $[O_2]$, the generation site for ROS (or something controlling it) may already be saturated, so adding more electrons cannot increase the rate any further. Therefore, in tissues, changes in the mix of substrates (complex I *versus* complex II) may or may not have a differential effect on ROS generation, depending on the prevailing $[O_2]$.

Notably, it has been observed that in skeletal muscle mitochondria, ROS generation under dual electron entry far exceeds the sum of rates with either complex I or complex II substrates alone (7). This may be due to different substrate preferences between muscle and liver mitochondria, which may in turn be related to differential expression levels of the various proteins of the oxidative phosphorylation machinery (35). Together, these results highlight that patterns of ROS generation vary greatly between different tissues and that tissue oxygenation is another factor that may influence specific pathways of mitochondrial ROS generation.

Effects of Inhibitors—The effect of mitochondrial inhibitors on ROS generation has been widely studied, but the influence of O_2 on these effects has not been. In the current investigation, two inhibitors, rotenone and antimycin A, were examined.

Rotenone binds at the downstream Q site within complex I, increasing ROS generation at the upstream FMN site. However, another effect of rotenone is to block electrons from exiting complex I and proceeding via the Q pool to complex III (27). Thus, rotenone decreases ROS generation from the complex III Q_O site. The effects of rotenone on overall ROS generation will manifest as a balance of these two effects, and herein we estimated that ROS generation at these two sites is differentially O_2-sensitive (Fig. 4, *A versus B*). Comparing the rates of ROS

FIGURE 4. **Estimated O_2 response of ROS generation rate at putative ROS-generating sites within the ETC.** Utilizing the data in Fig. 3, the amount of ROS generated for each of the following sites was calculated across a spectrum of $[O_2]$, as detailed under "Experimental Procedures" and calculated according to procedures outlined under "Discussion." *A*, the Q_O site of complex III. *B*, the FMN site of complex I. *C*, the backflow of electrons through complex I. *D*, the ETFQOR of β-oxidation. *E*, the comparison of ROS generation rates using substrates entering at complex I, complex II, or complexes I + II. *Inset*, ROS generation under these conditions at $[O_2]$ from 0 to 10 μM O_2. For data values obstructed by the *inset*, see Fig. 3 (conditions A, E, and H). *F*, the effect of rotenone on the response of mitochondrial ROS production to $[O_2]$ (*i.e.* data from Fig. 3*B* minus Fig. 3*A*). *G*, the effect of antimycin A on the response of mitochondrial ROS production to $[O_2]$ when respiring on succinate (*i.e.* data are reproduced from Fig. 3, *E* (*open symbols*) and *G* (*filled symbols*)).

generation in mitochondria respiring on complex I-linked substrates in the presence (condition B) and absence (condition A) of rotenone (*i.e.* subtracting A from B) reveals an interesting pattern for the effect of rotenone on ROS generation as a function of $[O_2]$ (Fig. 4*F*). At high $[O_2]$, rotenone stimulates ROS from the complex I FMN site, but it appears that rotenone-induced inhibition of ROS from the complex III Q_O site is insufficient to counteract this effect, and thus overall ROS generation increases. In contrast, at low $[O_2]$, although rotenone-stimulated ROS generation from the complex I FMN site still occurs, this is not enough to counteract the much larger decrease in ROS from the complex III Q_O site, so the net effect is an inhibition of ROS generation by rotenone. This effect may explain previous observations obtained by culturing cells at low $[O_2]$, in which rotenone inhibited ROS generation (36), compared with cells or isolated mitochondria at high $[O_2]$, in which rotenone stimulated ROS generation (5, 9, 31, 37, 38). These results highlight the critical importance of $[O_2]$ as a variable when using inhibitors to manipulate mitochondrial ROS.

The complex III inhibitor antimycin A has been widely used to augment ROS generation from the complex III Q_O site (6, 28, 39), but the effect of physiological variations in $[O_2]$ on this phenomenon has not been studied. The effect of antimycin A on ROS generation as a function of $[O_2]$ is shown in Fig. 4*G*, indicating that the -fold increase in ROS resulting from antimycin A addition is greater at high O_2 levels (3-fold at 20 μM O_2 *versus* 2-fold at 2 μM O_2). This is in agreement with a previous observation that the effect of antimycin A on mtROS was far greater under hyperoxic conditions (16). The reason underlying a lesser effect of antimycin A at lower $[O_2]$ may be diffusion limitation of O_2 availability at the Q_O site.

Physiological and Pathological Implications—Collectively, these data can aid in the understanding of mitochondrial function in disease states where $[O_2]$ may vary. One example is sepsis, in which the inflammatory response to infection elicits both hypoxia (40) and mitochondrial dysfunction (41). Treatment for sepsis usually includes antibiotics plus supplementary inhaled oxygen (*i.e.* 100% FiO_2) (42). Antibiotics have a number of adverse effects on mitochondrial function that may contribute to their organ-specific toxicities (43–46). Coupled with elevated $[O_2]$, such effects may enhance mtROS generation, which may contribute to pathology. Thus, enhanced knowledge about the complex interactions between the ETC, antibiotics, and $[O_2]$ may drive more careful selection of drugs to avoid excessive oxidative stress under 100% FiO_2.

In addition to hyperoxia, the current data may have implications for the role of mitochondria in cell signaling during hypoxia. Specifically, mitochondria within cells have been proposed to increase their ROS generation during hypoxia, leading to the stabilization of HIF-1α (hypoxia-inducible factor 1α) and the downstream expression of hypoxia-sensitive genes (47–51). The current data indicate that, under all of the metabolic conditions examined, mtROS decreased at low $[O_2]$.

Interestingly, the site of ROS generation that has received most attention within the context of hypoxic signaling is complex III (14). It is possible that the position of complex III in the respiratory chain adjacent to the terminal cytochrome *c* oxidase may render it more sensitive to redox events at the terminal oxidase (*e.g.* ischemia/hypoxia), compared with upstream complexes that are relatively more "cushioned" from such events (52). However, our results (Fig. 4) suggest that complex III is one of the least likely sites for ROS generation under hypoxic conditions. Thus, we hypothesize that in hypoxia, ROS may originate from an as yet unidentified mitochondrial source. Alternatively, since the current experiments highlight that the property of increased ROS in response to low O_2 is not autonomous to the mitochondrial respiratory chain, an additional signal external to the mitochondrion may be required to facilitate a hypoxic increase in mtROS within cells. Such a signal is probably absent from our isolated mitochondrial incubations. A third possibility is that differences in methodology (*e.g.* choice of fluorescent ROS probes) and definitions of "hypoxia" may account for the varied reports of hypoxic ROS generation in the literature (for discussion, see Ref. 15).

In summary, the data presented herein suggest that overall ROS generation by isolated mitochondria under a variety of metabolic conditions decreases at low $[O_2]$. Estimating the $[O_2]$ sensitivity of four putative ROS-generating sites within the ETC reveals a wide range of apparent K_m values. Thus, when considering the relative importance of these sites in contributing to overall mtROS generation and redox balance, it is essential to include $[O_2]$ as a variable. Finally, these data (see supplemental material) may facilitate the prediction of mtROS generation under a variety of metabolic conditions via incorporation into mathematical models of mitochondrial metabolism.

REFERENCES

1. Bayir, H., and Kagan, V. E. (2008) *Crit. Care* **12,** 206
2. Acker, H. (2005) *Philos. Trans. R. Soc. Lond. B Biol. Sci.* **360,** 2201–2210
3. Brookes, P. S., Yoon, Y., Robotham, J. L., Anders, M. W., and Sheu, S. S. (2004) *Am. J. Physiol. Cell Physiol.* **287,** C817–833
4. Chen, Q., Vazquez, E. J., Moghaddas, S., Hoppel, C. L., and Lesnefsky, E. J. (2003) *J. Biol. Chem.* **278,** 36027–36031
5. St-Pierre, J., Buckingham, J. A., Roebuck, S. J., and Brand, M. D. (2002) *J. Biol. Chem.* **277,** 44784–44790
6. Muller, F. L., Roberts, A. G., Bowman, M. K., and Kramer, D. M. (2003) *Biochemistry* **42,** 6493–6499
7. Muller, F. L., Liu, Y., Abdul-Ghani, M. A., Lustgarten, M. S., Bhattacharya, A., Jang, Y. C., and Van Remmen, H. (2008) *Biochem. J.* **409,** 491–499
8. Adam-Vizi, V., and Chinopoulos, C. (2006) *Trends Pharmacol. Sci.* **27,** 639–645
9. Lambert, A. J., and Brand, M. D. (2004) *J. Biol. Chem.* **279,** 39414–39420
10. Tsai, A. G., Johnson, P. C., and Intaglietta, M. (2003) *Physiol. Rev.* **83,** 933–963
11. Matsumoto, A., Matsumoto, S., Sowers, A. L., Koscielniak, J. W., Trigg, N. J., Kuppusamy, P., Mitchell, J. B., Subramanian, S., Krishna, M. C., and Matsumoto, K. (2005) *Magn. Reson. Med.* **54,** 1530–1535
12. Jones, D. P. (1986) *Am. J. Physiol. Cell Physiol.* **250,** C663–675
13. Takahashi, E., Sato, K., Endoh, H., Xu, Z. L., and Doi, K. (1998) *Am. J. Physiol. Heart Circ. Physiol.* **275,** H225–233
14. Guzy, R. D., and Schumacker, P. T. (2006) *Exp. Physiol.* **91,** 807–819
15. Hoffman, D. L., Salter, J. D., and Brookes, P. S. (2007) *Am. J. Physiol. Heart Circ. Physiol.* **292,** H101–108
16. Boveris, A., and Chance, B. (1973) *Biochem. J.* **134,** 707–716
17. Mairbaurl, H., Hotz, L., Chaudhuri, N., and Bartsch, P. (2005) *MiP 2005: Abstracts of the 4th Mitochondrial Physiology Meeting, Schroeken, Austria, September 16–20, 2005*, pp. 26–27, MiPNet Publications, Innsbruck, Austria
18. Michelakis, E. D., Hampl, V., Nsair, A., Wu, X., Harry, G., Haromy, A., Gurtu, R., and Archer, S. L. (2002) *Circ. Res.* **90,** 1307–1315
19. Campian, J. L., Qian, M., Gao, X., and Eaton, J. W. (2004) *J. Biol. Chem.*

279, 46580–46587
20. Aw, T. Y., Wilson, E., Hagen, T. M., and Jones, D. P. (1987) *Am. J. Physiol. Renal Physiol.* **253,** F440–447
21. Gnaiger, E. (ed) (2007) *Mitochondrial Pathways and Respiratory Control*, 2nd Ed., MiPNet Publications, Innsbruck, Austria
22. Brookes, P. S., Kraus, D. W., Shiva, S., Doeller, J. E., Barone, M. C., Patel, R. P., Lancaster, J. R., Jr., and Darley-Usmar, V. (2003) *J. Biol. Chem.* **278,** 31603–31609
23. Cole, R. P., Sukanek, P. C., Wittenberg, J. B., and Wittenberg, B. A. (1982) *J. Appl. Physiol.* **53,** 1116–1124
24. Rengasamy, A., and Johns, R. A. (1996) *J. Pharmacol. Exp. Ther.* **276,** 30–33
25. Wojtovich, A. P., and Brookes, P. S. (2008) *Biochim. Biophys. Acta* **1777,** 882–889
26. Pardee, A. B., and Potter, V. R. (1949) *J. Biol. Chem.* **178,** 241–250
27. Turrens, J. F., and Boveris, A. (1980) *Biochem. J.* **191,** 421–427
28. Sun, J., and Trumpower, B. L. (2003) *Arch. Biochem. Biophys.* **419,** 198–206
29. Sun, F., Huo, X., Zhai, Y., Wang, A., Xu, J., Su, D., Bartlam, M., and Rao, Z. (2005) *Cell* **121,** 1043–1057
30. Byun, H. O., Kim, H. Y., Lim, J. J., Seo, Y. H., and Yoon, G. (2008) *J. Cell. Biochem.* **104,** 1747–1759
31. Chen, Y., McMillan-Ward, E., Kong, J., Israels, S. J., and Gibson, S. B. (2007) *J. Cell Sci.* **120,** 4155–4166
32. Forquer, I., Covian, R., Bowman, M. K., Trumpower, B. L., and Kramer, D. M. (2006) *J. Biol. Chem.* **281,** 38459–38465
33. Gnaiger, E., Lassnig, B., Kuznetsov, A. V., and Margreiter, R. (1998) *Biochim. Biophys. Acta* **1365,** 249–254
34. Sperl, W., Skladal, D., Gnaiger, E., Wyss, M., Mayr, U., Hager, J., and Gellerich, F. N. (1997) *Mol. Cell Biochem.* **174,** 71–78
35. Johnson, D. T., Harris, R. A., Blair, P. V., and Balaban, R. S. (2007) *Am. J. Physiol. Cell Physiol* **292,** C698–707
36. Wang, Q. S., Zheng, Y. M., Dong, L., Ho, Y. S., Guo, Z., and Wang, Y. X. (2007) *Free Radic. Biol. Med.* **42,** 642–653
37. Chen, Q., Moghaddas, S., Hoppel, C. L., and Lesnefsky, E. J. (2008) *Am. J. Physiol. Cell Physiol.* **294,** C460–466
38. Barja, G. (1998) *Ann. N.Y. Acad. Sci.* **854,** 224–238
39. Boveris, A., Cadenas, E., and Stoppani, A. O. (1976) *Biochem. J.* **156,** 435–444
40. Goldman, D., Bateman, R. M., and Ellis, C. G. (2006) *Am. J. Physiol. Heart Circ. Physiol.* **290,** H2277–2285
41. Carré, J. E., and Singer, M. (2008) *Biochim. Biophys. Acta* **1777,** 763–771
42. Schuerholz, T., and Marx, G. (2008) *Minerva Anestesiol.* **74,** 181–195
43. Walker, P. D., and Shah, S. V. (1987) *Am. J. Physiol.* **253,** C495–499
44. Walker, P. D., Barri, Y., and Shah, S. V. (1999) *Ren. Fail.* **21,** 433–442
45. Dulon, D., Aurousseau, C., Erre, J. P., and Aran, J. M. (1988) *Acta Otolaryngol.* **106,** 219–225
46. Kroon, A. M., and Van den Bogert, C. (1983) *Pharm. Weekbl. Sci.* **5,** 81–87
47. Klimova, T., and Chandel, N. S. (2008) *Cell Death Differ.* **15,** 660–666
48. Bell, E. L., Klimova, T. A., Eisenbart, J., Moraes, C. T., Murphy, M. P., Budinger, G. R., and Chandel, N. S. (2007) *J. Cell Biol.* **177,** 1029–1036
49. Schroedl, C., McClintock, D. S., Budinger, G. R., and Chandel, N. S. (2002) *Am. J. Physiol. Lung Cell Mol. Physiol.* **283,** L922–931
50. Chandel, N. S., McClintock, D. S., Feliciano, C. E., Wood, T. M., Melendez, J. A., Rodriguez, A. M., and Schumacker, P. T. (2000) *J. Biol. Chem.* **275,** 25130–25138
51. Chandel, N. S., Maltepe, E., Goldwasser, E., Mathieu, C. E., Simon, M. C., and Schumacker, P. T. (1998) *Proc. Natl. Acad. Sci. U. S. A.* **95,** 11715–11720
52. Chance, B. (1965) *J. Gen. Physiol.* **49,** (suppl.) 163–195
53. National Research Council (1996) *Guide for Care and Use of Laboratory Animals*, National Institutes of Health Publication 86-23, National Institutes of Health, Bethesda, MD